Journal of Cell Science 110, 2141-2154 (1997)
Printed in Great Britain © The Company of Biologists Limited 1997
JCS9587

Interaction of *Bartonella henselae* with endothelial cells results in bacterial aggregation on the cell surface and the subsequent engulfment and internalisation of the bacterial aggregate by a unique structure, the invasome

Christoph Dehio[1,*], Marlene Meyer[1], Jürgen Berger[2], Heinz Schwarz[2] and Christa Lanz[1]

[1]Max-Planck-Institut für Biologie, Abteilung Infektionsbiologie, Spemannstraße 34, D-72076 Tübingen, Germany
[2] Max-Planck-Institut für Entwicklungsbiologie, Spemannstraße 36, D-72076 Tübingen, Germany

*Author for correspondence (e-mail: dehio@mpib-tuebingen.mpg.de)

SUMMARY

Vascular colonisation by *Bartonella henselae* may cause vaso-proliferative tumour growth with clumps of bacteria found in close association with proliferating endothelial cells. By using *B. henselae*-infected human umbilical vein endothelial cells as an in vitro model for endothelial colonisation, we report here on a novel mechanism of cellular invasion by bacteria. First, the leading lamella of endothelial cells establishes cellular contact to sedimented bacteria and mediates bacterial aggregation by rearward transport on the cell surface. Subsequently, the formed bacterial aggregate is engulfed and internalised by a unique host cellular structure, the invasome. Completion of this sequence of events requires 24 hours. Cortical F-actin, intercellular adhesion molecule-1 and phosphotyrosine are highly enriched in the membrane protrusions entrapping the bacterial aggregate. Actin stress fibres, which are anchored to the numerous focal adhesion plaques associated with the invasome structure, are typically found to be twisted around its basal part. The formation of invasomes was found to be inhibited by cytochalasin D but virtually unaffected by nocodazole, colchicine or taxol, indicating that invasome-mediated invasion is an actin-dependent and microtubuli-independent process. Bacterial internalisation via the invasome was consistently observed with several clinical isolates of *B. henselae*, while a spontaneous mutant obtained from one of these isolates was impaired in invasome-mediated invasion. Instead, this mutant showed increased uptake of bacteria into perinuclear localising phagosomes, suggesting that invasome-formation may interfere with this alternative mechanism of bacterial internalisation. Internalisation via the invasome represents a novel paradigm for the invasion of bacteria into host cells which may serve as a cellular colonisation mechanism in vivo, e.g. on proliferating and migrating endothelial cells during *Bartonella*-induced vaso-proliferative tumour growth.

Key words: *Bartonella henselae*, Endothelial cell, Cell invasion

INTRODUCTION

Bartonella (Rochalimaea) henselae is a newly recognised fastidious gram-negative bacillus (Regnery et al., 1992; Brenner et al., 1993) that has been associated with an increasing number of clinical manifestations in human infection, including bacillary angiomatosis, parenchymal bacillary peliosis, cat scratch disease, persisting bacteremia and endocarditis (for review see Adal et al., 1994). Bacillary angiomatosis, which is seen primarily among immunocompromised patients, is characterised by the formation of skin tumours which clinically resemble the Kaposi sarcoma (for review see Koehler and Tappero, 1993; Adal et al., 1994). Histological studies have indicated a vaso-proliferative origin for these tumours, with clumps of bacteria found in close association with the proliferating endothelial cells which line up to form new capillaries (Schneider et al., 1993; Hettmansperger et al., 1993; Monteil et al., 1994). This angiogenic process is likely to be stimulated by bacterial factors, since in vitro studies have demonstrated migration and proliferation of endothelial cells in response to infection with *B. henselae* (Conley et al., 1994). Bacterial colonisation of the tumour lesions is critical for tumorous growth, since bacterial eradication by antibiotic treatment results in complete tumour regression (Webster et al., 1992; reviewed by Koehler and Tappero, 1993), yet little is known about the mechanisms by which *B. henselae* colonises endothelial cells. Invasion of cultured epithelial cells by *B. henselae* correlates with cell adherence mediated by the expression of type 4-like pili (Batterman et al., 1995). Adherent bacteria are internalised within hours by a cytochalasin D-sensitive invasion process (Batterman et al., 1995) giving rise to intracellular bacteria residing within perinuclear phagosomes (Zbinden et al., 1995). Using cultured human umbilical vein endothelial cells (HUVECs) as an infection model, we describe here a novel mechanism for bacterial uptake into mammalian cells. We have applied immunocytochemistry, various microscopic techniques and inhibitors of cytoskeletal functions to characterise the sequence of host cell-pathogen interactions

leading to the formation of the invasome. This unique, actin-dependent structure mediates the internalisation of a large bacterial aggregate, a mechanism which may allow the colonisation of vascular tissues in vivo.

MATERIALS AND METHODS

Cell lines and bacterial strains

HUVECs were isolated from the vein of fresh human umbilical cords. The vein was thoroughly washed with buffer containing 150 mM NaCl, 5 mM KCl, 4 mM $NaHCO_3$ and 5 mM D-glucose, pH 7.3, before incubation with 50 μg/ml α-chymotrypsin (Sigma, Deisenhofen, Germany) in phosphate buffered saline for 15 minutes at 37°C. The solution recovered from the lumen of the vein was centrifuged for 5 minutes at 2,800 ***g***, and the pelleted cells were resuspended in medium 199 (Life Technologies, Eggenstein, Germany) supplemented with 10% heat-inactivated fetal calf serum (FCS, Boehringer Mannheim, Mannheim, Germany) and seeded onto plastic coated with 0.2% gelatin (Sigma, Deisenhofen, Germany). Following incubation for several hours in a humidified atmosphere at 37°C and 5% CO_2 to allow spreading of endothelial cells, erythrocytes and non-adherent cells were washed off the monolayers with fresh medium, and cells were grown for up to 8 passages in endothelial growth medium (EGM, Promocell, Heidelberg, Germany).

Bartonella henselae strains ATCC 49793, OK88-674, OK90-615 (Welch et al., 1992), ATCC 49882 (Regnery et al., 1992) and San Ant-1 (Lucey et al., 1992), which were previously isolated from human blood and strain 49882 Rif, a spontaneous Rif-resistant mutant of ATCC 49882 (Dehio and Meyer, 1997), were all grown on Columbia agar (Difco Laboratories, Detroit, MI, USA) supplemented with 5% defibrinated sheep blood agar (Difco Laboratories, Detroit, MI, USA) in a humidified atmosphere at 37°C and 5% CO_2.

Infection assays

HUVECs (passages 3 to 8) were seeded the day before the experiment in medium 199/10% heat-inactivated FCS on coverslips coated with 0.2% gelatine and placed inside individual wells of a 24-well cell culture plate (Costar, Cambridge, MA, USA). For infection, bacteria harvested from a 3 days grown plate were suspended in medium 199/10% FCS to an OD_{550nm} = 0.01 and 1 ml of this suspension was added per well. Bacteria were then sedimented onto the cultured cells by centrifugation for 5 minutes at 1,800 ***g***. Infected cell cultures were maintained in a humidified atmosphere at 37°C and 5% CO_2 and the medium was replaced next day to prevent bacterial overgrowth. When indicated, nocodazole, colchicine, taxol or cytochalasine D (all from Sigma, Deisenhofen, Germany) were added together with the bacteria and maintained throughout the infection. Infection was stopped at the time indicated by three washes in phosphate buffered saline supplemented with 1 mM $CaCl_2$ and 0.5 mM $MgCl_2$ and cells were fixed in 3.7% formaldehyde (prepared by depolymerisation of paraformaldehyde) in 200 mM Hepes, pH 7.4, for at least 30 minutes at room temperature.

Antibodies

Rabbit polyclonal antibodies (serum 2037) were raised against formalin-fixed whole bacteria of *B. henselae* strain ATCC 49882. Mouse monoclonal anti-phosphotyrosine antibodies, clone 4G10, were purchased from Upstate Biotechnology Inc. (Lake Placid, NY, USA). Mouse monoclonal anti-ICAM-1 antibodies, clone 6.5B5, were a gift from Dr D. Haskard (Hammersmith Hospital, London, UK). Mouse monoclonal anti-α-tubulin antibodies were purchased from Amersham (Buckinghamshire, UK). Mouse monoclonal anti-LAMP-1 antibodies, clone H4A3, was obtained from the Developmental Studies Hybridoma Bank (University of Iowa, Iowa City, IA, USA). Texas Red-conjugated goat anti-mouse IgG antibodies were purchased from Dianova (Hamburg, Germany) and Cy5-conjuated goat anti-rabbit IgG antibodies were purchased from Jackson ImmunoResearch Laboratories (West Grove, PA, USA). Nanogold-conjugated goat-anti mouse IgG antibodies were purchased from Nanoprobes (Stony Brook, NY, USA) and FITC-labelled phalloidin was purchased from Sigma (Deisenhofen, Germany).

Immunofluorescence labelling and immunogold labelling

For all staining protocols, the formaldehyde-fixed cells were washed three times in phosphate buffered saline at the beginning and following each incubation step. For differential staining of intracellular and extracellular bacteria, fixed cells were sequentially incubated with 0.2% BSA in phosphate buffered saline for 15 minutes to block unspecific binding, rabbit anti-*B. henselae* antiserum (diluted 1/100 in phosphate buffered saline) for 1 hour, Texas Red-conjugated goat anti-rabbit IgG antibodies (diluted 1/100 in phosphate buffered saline) for 1 hour, 0.1% Triton X-100 in phosphate buffered saline for 15 minutes, 0.2% of BSA in phosphate buffered saline for 15 minutes, rabbit anti-*B. henselae* antiserum (diluted 1/100 in phosphate buffered saline) for 1 hour and Cy5-conjugated goat anti-rabbit antibodies mixed with FITC-labelled phalloidin (diluted 1/100 or to 1 μg/ml in phosphate buffered saline, respectively) for 1 hour. For triple staining of bacteria, F-actin and an additional cellular component, fixed cells were sequentially incubated with 0.1% of Triton X-100 in phosphate buffered saline for 15 minutes, 0.2% of BSA in phosphate buffered saline for 15 minutes, mouse monoclonal antibodies directed against either ICAM-1, phosphotyrosine, α-tubulin, or LAMP-1 (each diluted 1/100 in phosphate buffered saline) for 1 hour, Texas Red-conjugated goat anti-mouse IgG antibodies (diluted 1/100 in phosphate buffered saline) for 1 hour, rabbit anti-*B. henselae* antiserum (diluted 1/100 in phosphate buffered saline) for 1 hour and Cy5-conjugated goat anti-rabbit IgG antibodies mixed with FITC-labelled phalloidin (diluted 1/100 or to 1 μg/ml in phosphate buffered saline, respectively) for 1 hour. Stained specimens were mounted in 100 mM Tris-HCl, pH 8.5, 25% glycerol (w/v) and 10% Moviol 4-88 (w/v, Hoechst, Frankfurt, Germany). For pre-embedding immunogold labelling, coverslips with formaldehyde-fixed cells were sequentially incubated with 0.1% of Triton X-100 in phosphate buffered saline for 15 minutes, 0.2% of BSA in phosphate buffered saline for 15 minutes, mouse monoclonal antibodies directed against ICAM-1 (diluted 1/100 in phosphate buffered saline) for 1 hour and Nanogold-conjugated goat anti-mouse IgG antibodies (diluted 1/100 in phosphate buffered saline) for 1 hour prior to silver enhancement (Danscher, 1981) for 25 minutes and further processing for SEM or TEM.

Confocal laser scanning microscopy and quantification of invasome stages

The samples stained for immunofluorescence were viewed with a Leica TCS NT confocal laser scanning microscope (Leica Lasertechnik, Heidelberg, Germany) equipped with an argon/krypton mixed gas laser. In triple stainings, the three channels were recorded simultaneously. The corresponding images were digitally processed with Photoshop 4.0 (Adobe Systems, Mountain View, CA).

To quantify invasomes, infected HUVECs differentially stained for extracellular and intracellular bacteria and for F-actin were viewed by continuous scanning. Randomly chosen cells (n=50) were examined for the presence of three sequential invasome stages: (i) bacterial aggregates on the cell surface not associated with membrane protrusions; (ii) bacterial aggregates engulfed by membrane protrusions but still accessible to antibodies before membrane permeabilisation (incomplete invasome); and (iii) bacterial aggregates internalised into the host cells and therefore accessible to antibodies only after membrane permeabilisation (complete invasome). Results are expressed for each of the invasome stages as mean and standard deviation of at least two independent determinations.

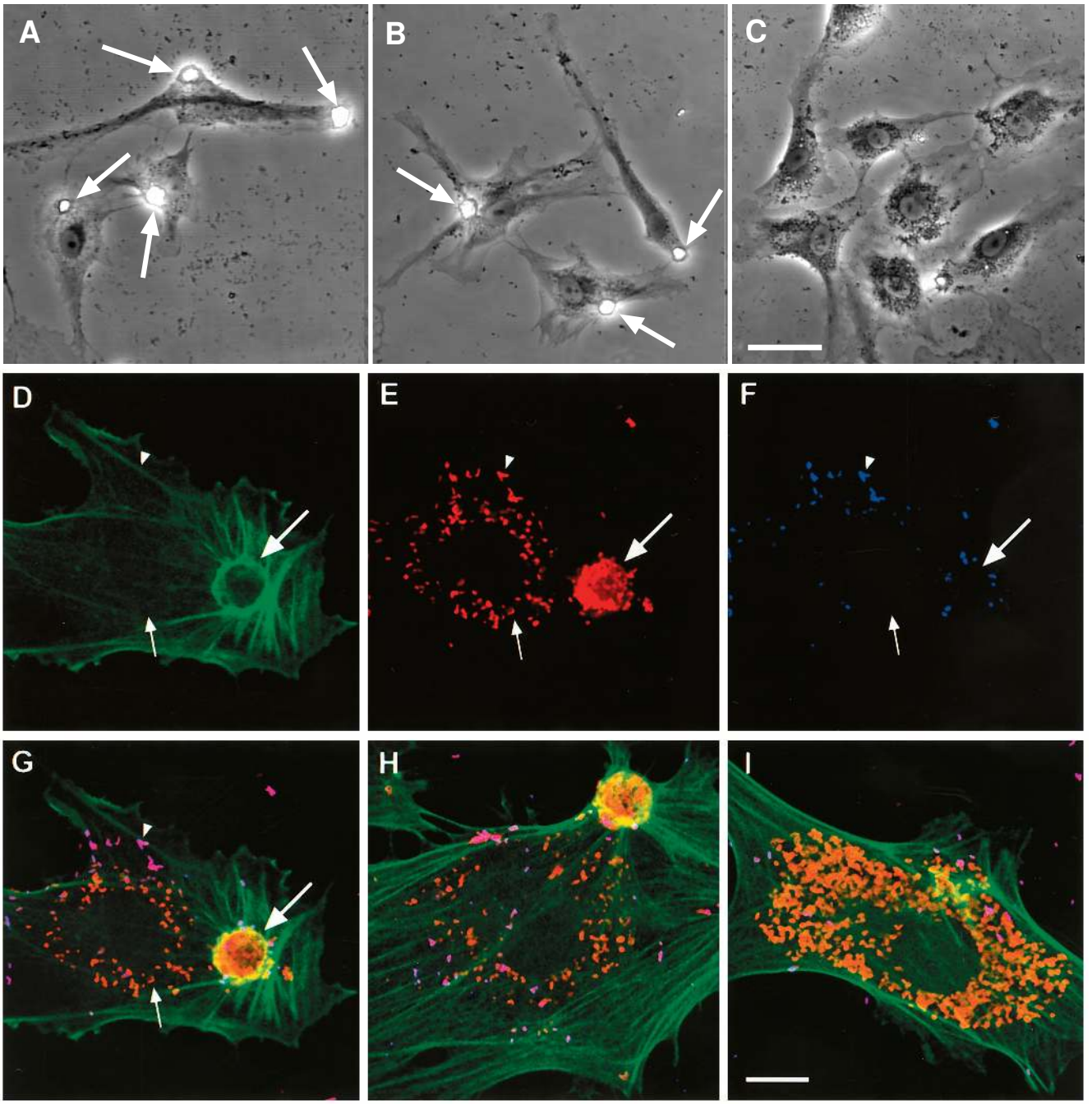

Fig. 1. Infection of human umbilical vein endothelial cells (HUVECs) with *B. henselae* results in the formation of the invasome, a cellular structure involved in the internalisation of a bacterial aggregate. HUVECs were infected with *B. henselae* strains ATCC 49793 (A, D-G), ATCC 49882 (B,H), or 49882 Rif (C,I) for 48 hours, washed and fixed with formaldehyde. Phase contrast pictures were taken (A-C, arrows point to invasomes) or specimens were immunocytochemically stained for extracellular bacteria, intracellular bacteria and the actin cytoskeleton and analysed by confocal laser scanning microscopy (D-I). Prior to the permeabilisation of the host cell membranes, extracellular bacteria were labelled with anti-*B. henselae* antiserum and Texas Red-conjugated secondary antibodies (F, blue channel). Following permeabilisation, the totality of bacteria was labelled with anti-*B. henselae* antiserum and Cy5-conjugated secondary antibodies (E). The actin cytoskeleton was stained with FITC-labelled phalloidin in order to indicate the location of cellular structures (D). The overlay of all three channels is represented in G. Intracellular bacteria appear in red due to the absence of a signal in the blue channel, or, in the case of a co-localisation with F-actin staining, in yellow. In contrast, extracellular bacteria appear purple as a result of the superimposition of signals both in the red channel and the blue channel. The position of a representative example for extracellular bacteria (arrowheads), intracellular bacteria residing within perinuclear endosomes (small arrows) and the bacterial aggregate within the invasome structure (large arrows) are marked in the three separate channels and the respective overlay (D-G). Bars: 50 µm (A-C) ; 10 µm (D-I).

Electron microscopy

For transmission electron microscopy (TEM), formaldehyde-fixed cells were post-fixed with 1% osmium tetroxide in phosphate buffered saline for 1 hour on ice and, after rinsing with double distilled water, treated with 1% aqueous uranyl acetate for 1 hour at 4°C. If cells had been previously stained by silver-enhanced immunogold-labelling, the uranyl acetate treatment was omitted. Samples were dehydrated through a graded series of ethanol and embedded in Epon. Ultrathin sections were stained with uranyl acetate and lead citrate and viewed in a Philips CM10 electron microscope. For scanning electron microscopy (SEM), gold-labelled cells were fixed with 1% glutaraldehyde, post-fixed with 1% osmium tetroxide in phosphate-buffered saline, dehydrated in ethanol and critical-point-dried from CO_2. The samples were sputter-coated with 1 nm chromium and examined at 10 kV accelerating voltage in a Hitachi S-800 field emission scanning electron microscope equipped with a detector for backscattered electrons (BSE) of the YAG type (Autrata et al., 1992).

Time-lapse microcinematography and phase contrast microscopy

Time-lapse phase contrast images of HUVECs infected with *B. henselae* were recorded every 30 minutes by scanning phase contrast images in the transmission channel of a Leica TCS NT confocal laser scanning microscope. The microscope stage was heated to 37°C and the medium was regularly replaced with fresh 5% CO_2-equilibrated medium.

RESULTS

Infection of human umbilical vein endothelial cells with *B. henselae* results in the formation of the invasome, a unique structure involved in the internalisation of a bacterial aggregate

As infection with *B. henselae* may result in vascular colonisation in vivo, we have used HUVECs as an infection model to study mechanisms of endothelial colonisation in vitro. *B. henselae* is a slow growing fastidious bacterium, that can be co-cultivated with cultured mammalian cells for extended periods of time. We have observed that within 24 hours of infection of HUVECs with *B. henselae,* a unique structure, which we have termed the invasome, is formed. By means of phase contrast light microscopy, the typical appearance of the invasome is a solitary, globular structure of 5 to 15 µm in diameter which is normally found at a distal location relative to the cell nucleus (Fig. 1A,B, arrows). Invasome formation was observed with several clinical isolates of *B. henselae*, ATCC 49793 (Fig. 1A; Welch et al., 1992), ATCC 49882 (Fig. 1B; Regnery et al., 1992), San Ant-1 (Lucey et al., 1992, data not shown), OK88-674 and OK-615 (Welch et al., also data not shown). However, a mutant strain obtained from ATCC 49882, 49882 Rif (Fig. 1C), was found to be impaired in invasome formation, suggesting that the formation of invasomes is dependent on the expression of specific bacterial determinants. This mutant was originally isolated by its spontaneous resistance to rifampicin (Dehio and Meyer, 1997), while the deficiency in invasome-mediated internalisation was found coincidentally.

In order to study the spatial relationship of bacteria and cellular structures, an immunocytochemical staining protocol differentially labelling extracellular and intracellular bacteria as well as cellular structures was used in combination with confocal laser scanning microscopy. Extracellular bacteria were labelled with antiserum and secondary Texas Red-conjugated antibodies (Fig. 1F) prior to the permeabilisation of the host cell membrane and labelling of the totality of bacteria with antiserum and secondary Cy5-conjugated antibodies (Fig. 1E). To localise the invasome structure formed by the induced cytoskeletal rearrangements, the actin cytoskeleton was stained

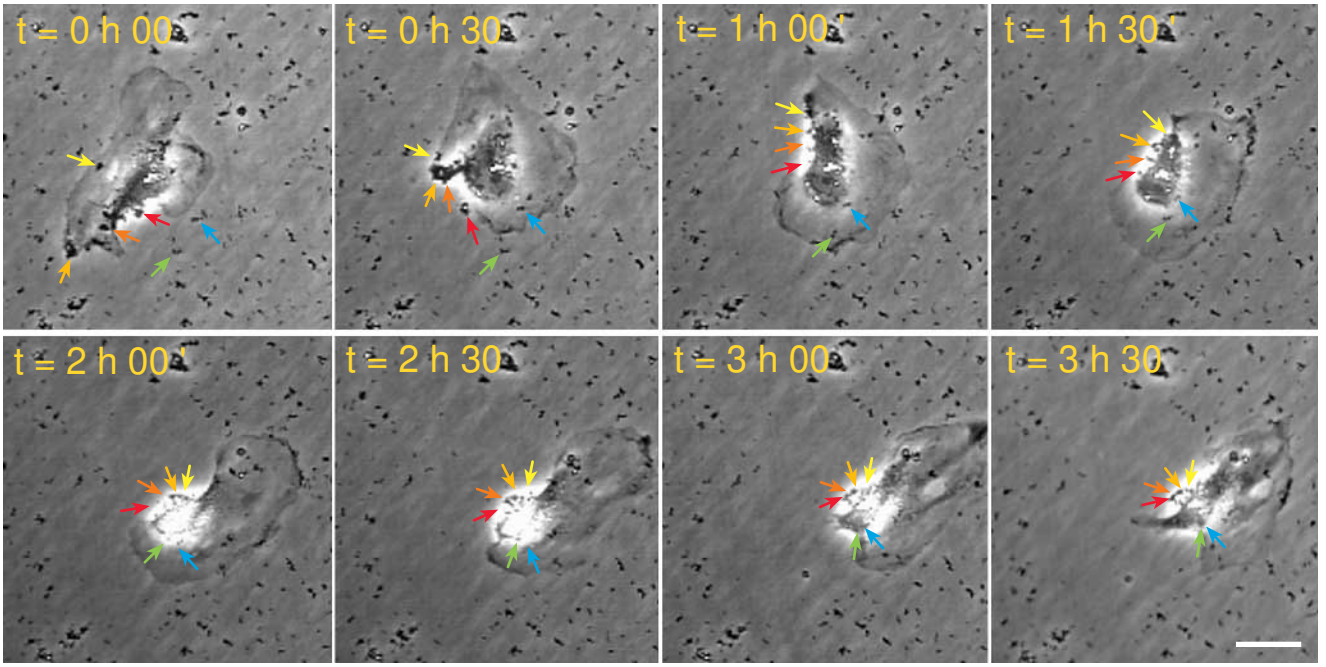

Fig. 2. Time-lapse microcinematography of the interaction of HUVECs with *B. henselae*. *B. henselae* ATCC 49793 was centrifuged onto a monolayer of HUVECs and phase contrast images were taken at intervals of 30 minutes. The total infection time (t) is indicated for each picture. Individual or small clusters of bacteria are marked by arrows of the same colour. Bar, 10 µm.

with FITC-labelled phalloidin (Fig. 1D). In the overlay of all three channels (Fig. 1G), intracellular bacteria appear in red (a representative example is marked by a small arrow in Fig. 1D-G) or, in the case of a co-localisation with F-actin staining, in yellow, while extracellular bacteria appear purple (a representative example is marked by an arrowhead in Fig. 1D-G). By this technique, we could demonstrate for strain ATCC 49793 that: (i) the induced invasome structure can be recognised by a marked rearrangement of the actin cytoskeleton (Fig. 1D,G, large arrow), and (ii) the invasome contains a large and completely internalised bacterial aggregate (Fig. 1E-G, large arrow). An indistinguishable staining pattern was seen for HUVECs infected with strain ATCC 49882 (3-channel overlay in Fig. 1H), while infection with the isogenic mutant strain 49882 Rif did not reveal invasomes (3-channel overlay in Fig. 1I).

In addition to invasome-mediated internalisation, we have also observed an alternative mechanism of *B. henselae* invasion into HUVECs. In this instance, intracellular *B. henselae* are found to reside within perinuclear phagosomes (unpublished results). Interestingly, invasome-mediated internalisation appears to interfere with this alternative invasion mechanism. Strain 49882 Rif, which is impaired in invasome-mediated invasion, showed increased rates of bacterial internalisation by this alternative process of cell invasion (Fig. 1I) when compared to the invasome-forming isogenic strain ATCC 49882 (Fig. 1H) or the independent clinical isolate ATCC 49793 (Fig. 1D-G, small arrow). These perinuclear localised intracellular bacteria can already be recognised as black granules in phase contrast images (Fig. 1A-C), again suggesting a different mechanism of bacterial uptake for strain 49882 Rif (Fig. 1C) when compared to ATCC49882 (Fig. 1B) and ATCC49793 (Fig. 1A). It is important to note that the totality of intracellular bacteria is roughly the same for all three strains tested, indicating that the impairment of strain 49882 Rif for invasome-mediated internalisation is not a result of impairment

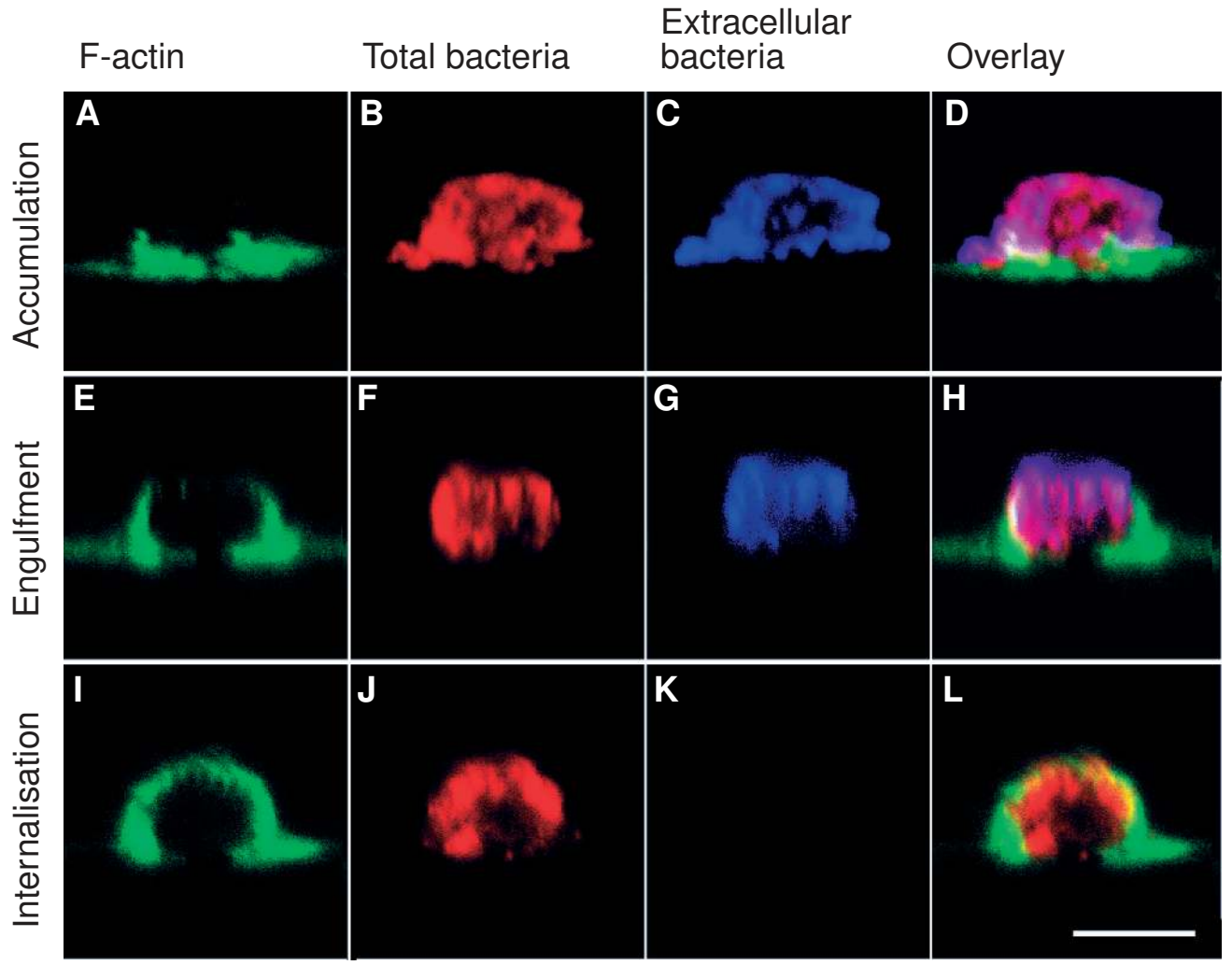

Fig. 3. Confocal analysis of invasome-mediated invasion. HUVECs were infected with *B. henselae* strain ATCC 49793 for 18 hours (A-D), 24 hours (E-H) or 30 hours (I-L), washed and fixed with formaldehyde. Specimens were stained for extracellular bacteria (before permeabilisation, blue channel in C,G,K) or the totality of bacteria (after permeabilisation, red channel in B,F,J) by indirect immunofluorescence staining and filamentous actin was stained by FITC-labelled phalloidin (green channel in A,E,I) and specimens were analysed by *x-z* sectioning in confocal laser scanning microscopy. An overlay of all three channels is represented in D,H,L. The formation (A-D), engulfment (E-H) and internalisation (I-L) of a bacterial aggregate represent sequential stages in the process of invasome-mediated internalisation. Bar, 10 μm.

in establishing interaction with the host cell, but rather reflects differences in the bacterial uptake mechanisms provoked by the established interactions.

Invasome-mediated internalisation involves the accumulation and aggregation of *B. henselae* on the cell surface, a process which is mediated by movement of the leading lamella

A large, evenly round bacterial aggregate is always found to be associated with the invasome structure, suggesting that bacterial accumulation and aggregation on the cell surface may precede the formation of an invasome. Time-lapse microcinematography indicated that movement of the leading lamella of the endothelial cell establishes cell surface interaction with bacteria sedimented onto the culture substratum (Fig. 2). The absence of bacteria from the culture substratum in an area surrounding any infected endothelial cells (Fig. 2, compare t=0 minutes with any later time point of infection) reflects the movement of endothelial cells and the efficiency in mediating cell surface interactions with the encountered bacteria. Subsequent to the establishment of interaction with the leading lamella, bacteria are transported rearward across the leading lamella to a site just ahead of the nucleus, resulting in the formation of a cell surface associated bacterial aggregate (Fig. 2, individual bacteria or bacterial clusters are marked by arrows of the same colour). Once an invasome is formed, the endothelial cell appears to move less actively, while the leading edge still mediates interactions with bacteria sedimented onto the substratum in the cellular vicinity and rearward transport mechanisms mediate movement of interacting bacteria towards the invasome (data not shown).

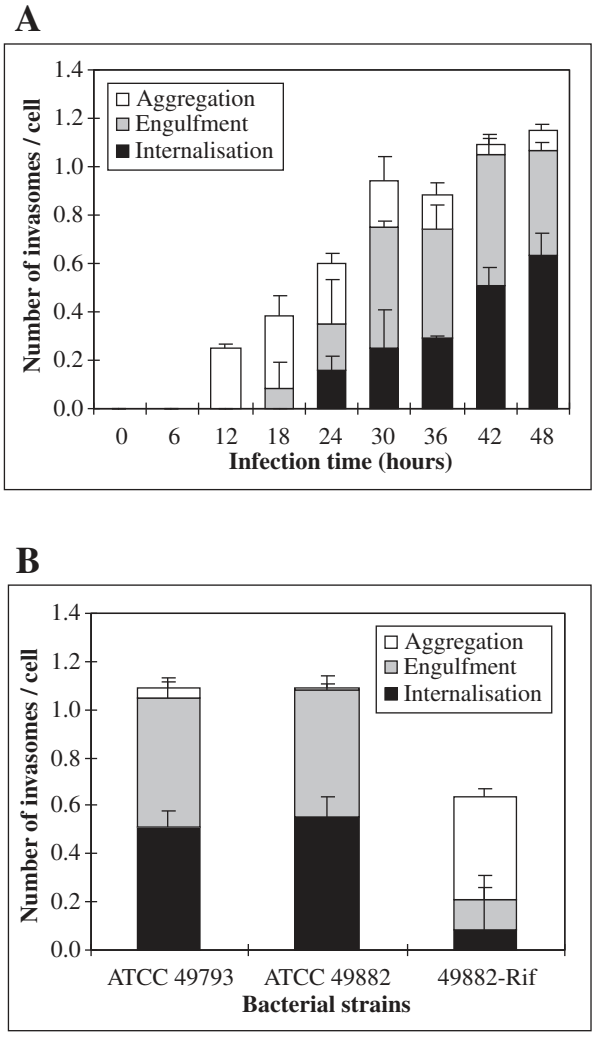

Fig. 4. Time- and strain-dependency of invasome-mediated invasion. HUVECs were infected with the *B. henselae* strain ATCC 49793 for various periods of time as indicated (A) or with the strains ATCC 49793, ATCC49882 or 49882 Rif for 42 hours (B) and the frequencies of three sequential stages of the invasome structure, the (i) formation, (ii) engulfment, and (iii) internalisation of a bacterial aggregate were quantified as described in Materials and Methods.

Bacterial aggregation, and the subsequent engulfment and internalisation of the bacterial aggregate by membrane protrusions represent sequential stages in the process of invasome-mediated invasion

To characterise the order of events in the process of invasome-mediated invasion in more detail, we have performed a time-course of infection of HUVECs with *B. henselae* strain ATCC 49793. Fixed cells were stained immunocytochemically for intracellular and extracellular bacteria as well as for F-actin to visualise the cytoskeletal rearrangements resulting from invasome-formation (as described above for Fig. 1). Stained specimens were analysed by confocal microscopy taking optical sections in the *x-z* plane of the invasome structure. Three sequential stages of invasome-formation could be distinguished based upon morphological criteria (Fig. 3) and their relative frequency of appearance at various time-points of infection (see Fig. 4A). The earliest of these stages is represented by a cell surface-located bacterial aggregate which may or may not be associated with F-actin rearrangements (Fig. 3A-D). The second stage is marked by a partial engulfment of the bacterial aggregate by membrane protrusions, which show a strong staining for submembranous F-actin (Fig. 3E,H). At this stage, bacteria are still accessible to antibodies before host cell membrane permeabilisation (Fig. 3, compare G,H), indicating that they are extracellularly located. In the final stage, the bacterial aggregate is found to be internalised into the cell (Fig. 3I-L). Complete internalisation is indicated by the inaccessibility of bacteria to antibodies before host cell membrane permeabilisation (Fig. 3, compare J,K) and by the intense F-actin staining circumscribing the bacterial aggregate (Fig. 3I,L).

As shown in Fig. 4A, bacterial aggregation is observed first after 12 hours (aggregation stage), partially developed invasomes (engulfment stage) appear first at 18 hours and completed invasomes (internalisation stage) appear at 24 hours. All three invasome stages coexist at 24 hours and later time points, with the relative proportions shifting towards completion of the invasome structure. Almost any cell is associated with an invasome structure at 42 hours. In conclusion, invasome-mediated invasion is a prevalent phenomenon taking about 1 day for completion.

The clinical isolates ATCC 49793 and ATCC 49882 show the same capacity for invasome-mediated invasion as indicated by the frequency of the three sequential invasome stages determined at 42 hours post infection (Fig. 4B). The mutant strain 49882 Rif accumulates on the cell surface while aggregate

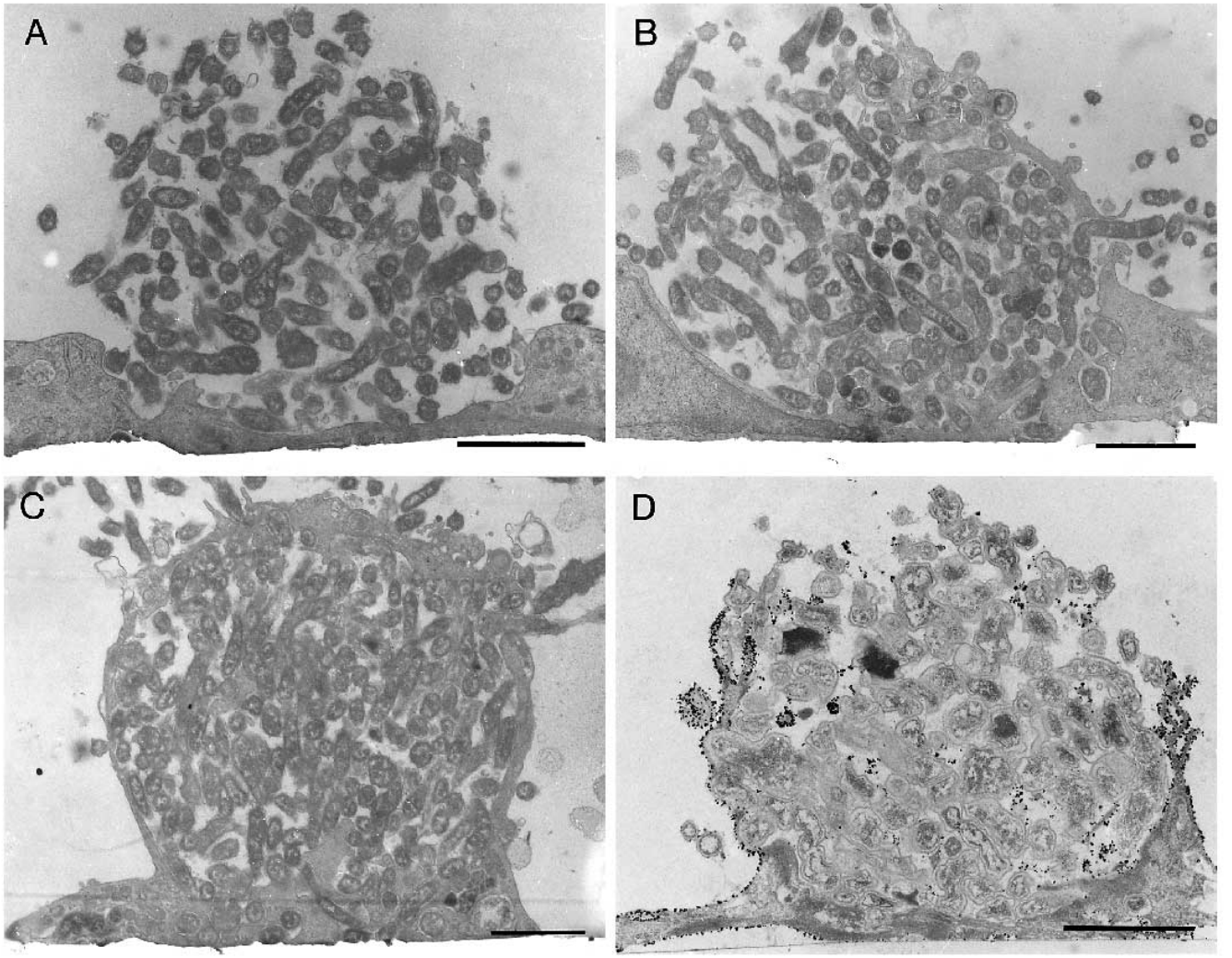

Fig. 5. TEM analysis of invasome-mediated invasion. HUVECs were infected with *B. henselae* strain ATCC 49793 for 48 hours, washed and fixed with formaldehyde. Specimens were processed for TEM, including a pre-embedding immunogold-labelling with monoclonal anti-ICAM-1 antibodies in D. The formation (A), engulfment (B,D) and internalisation (C) of a bacterial aggregate represent sequential stages in the process of invasome-mediated internalisation. Bars, 2 μm.

engulfment and internalisation is blocked. In contrast to cell surface-located aggregates of ATCC 49793 and ATCC 49882, aggregates of 49882 Rif are normally not associated with F-actin rearrangements, suggesting that this mutant is unable to provoke cytoskeletal rearrangements.

The described sequential stages of invasome-mediated internalisation were further analysed on the ultrastructural level by transmission electron microscopy (TEM, Fig. 5) and scanning electron microscopy (SEM, Fig. 6). Silver-enhanced immunogold-labelling of cell surface-located intercellular adhesion molecule-1 (ICAM-1) was used in SEM (Fig. 6) and in one instance in TEM (Fig. 5D), which unequivocally allowed to differentiate between labelled cell surface structures and unlabelled bacteria. In SEM, images of secondary electrons (SE, Fig. 6A,C,E), which show the normal morphology as well as images of back scattered electrons (BSE, Fig. 6B,D,F), which highlight the silver-enhanced gold grains, were both parallelly recorded. At the stage of bacterial aggregation, no membrane protrusions are evident (Fig. 5A) or may entrap only individual bacteria directly interacting with the cell surface (Fig. 6A,B). Engulfment of the bacterial aggregate appears to result from a circular outgrowth of membrane protrusions from the cell contact area with the bacterial aggregate (Fig. 5B,D). The membrane protrusions formed are very thin and appear to be firmly associated with the underlying bacteria. Once membrane protrusions extend to the top of the bacterial aggregate (Fig. 6C,D), they appear to finally fuse with each other resulting in the complete internalisation of the bacterial aggregate (Fig. 5C and 6E,F). At this stage, the bacterial aggregate is separated from the extracellular medium by a contiguous thin layer of two cellular membranes containing little cytoplasm in between.

The membrane protrusions of the invasome engulfing the bacterial aggregate are enriched for ICAM-1, submembranous F-actin and phosphotyrosine

By means of immunogold-labelling of ICAM-1 in TEM (Fig. 5D) and SEM (Fig. 6C,D), this surface marker was found to

be enriched in membrane protrusions of the invasome, in particular in the tips of the protrusions which firmly associate with the underlying bacterial aggregate. We confirmed this distribution of ICAM-1 by indirect immunocytochemical staining and confocal microscopy. The invasome structure illustrated in Fig. 7A-L is at an incomplete stage, similar to that shown in Fig. 6C,D, while Fig. 7M-P illustrates a completed invasome similar to that shown in Fig. 6E,F. Compared to the level of ICAM-1 staining on the cell surface (Fig. 7B), the staining is strongly increased on the membrane protrusions (Fig. 7F) including their tips (Fig. 7J, arrow). Submembranous F-actin is also enriched in the membrane protrusions and colocalises with ICAM-1 (Fig. 7E,H) except for the tips of the membrane protrusions (Fig. 7I,L, arrow).

Phosphotyrosine was also enriched in the membrane protrusions of the invasome (Fig. 8E), where it colocalises with submembranous F-actin (Fig. 8D,F). Phosphotyrosine distributes primarily to focal adhesion plaques in other parts of the cell (Fig. 8B,C, arrowheads) similar as in uninfected cells (data not shown).

Firm attachment of the invasome to the cell substratum is indicated by stress fibres, which are twisted around the basal part of the invasome and are anchored to closely associated focal adhesion plaques

TEM analysis of the invasome structure indicates that little cellular material resides in between the bacterial aggregate and the cell substratum (Fig. 5). Microtubuli and endocytic compartments staining positive for lysosome associated membrane protein-1 (LAMP-1) were found to be excluded from this space as shown by confocal microscopy (see Fig. 9G and data not shown). Instead, the basis of the invasome typically exhibits a

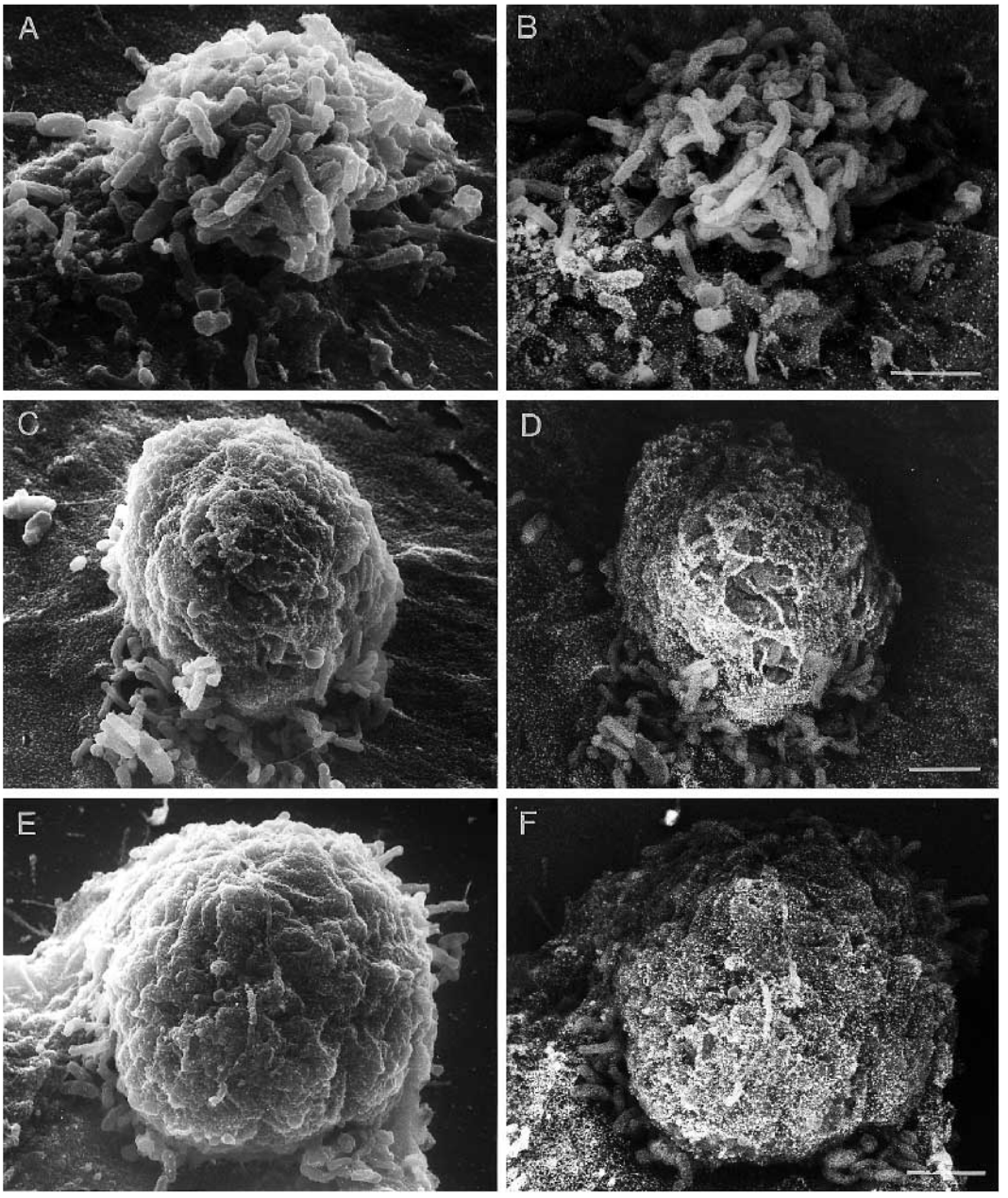

Fig. 6. SEM analysis of invasome-mediated invasion. HUVECs were infected with *B. henselae* strain ATCC 49793 for 48 hours, washed and fixed with formaldehyde. Specimens were stained for ICAM-1 by silver-enhanced immunogold labelling and processed for SEM. SE (secondary electrons in A,C,E) and BSE (back scattered electrons in B,D,F) illustrations are presented in parallel. The SE picture illustrates the surface topology, while the BSE pictures highlight specifically the silver-enhanced gold grains resulting from immunogold-labelling of ICAM-1. The formation (A,B), engulfment (C,D) and internalisation (E,F) of a bacterial aggregate represent sequential stages in invasome-mediated invasion. Bars, 2 μm.

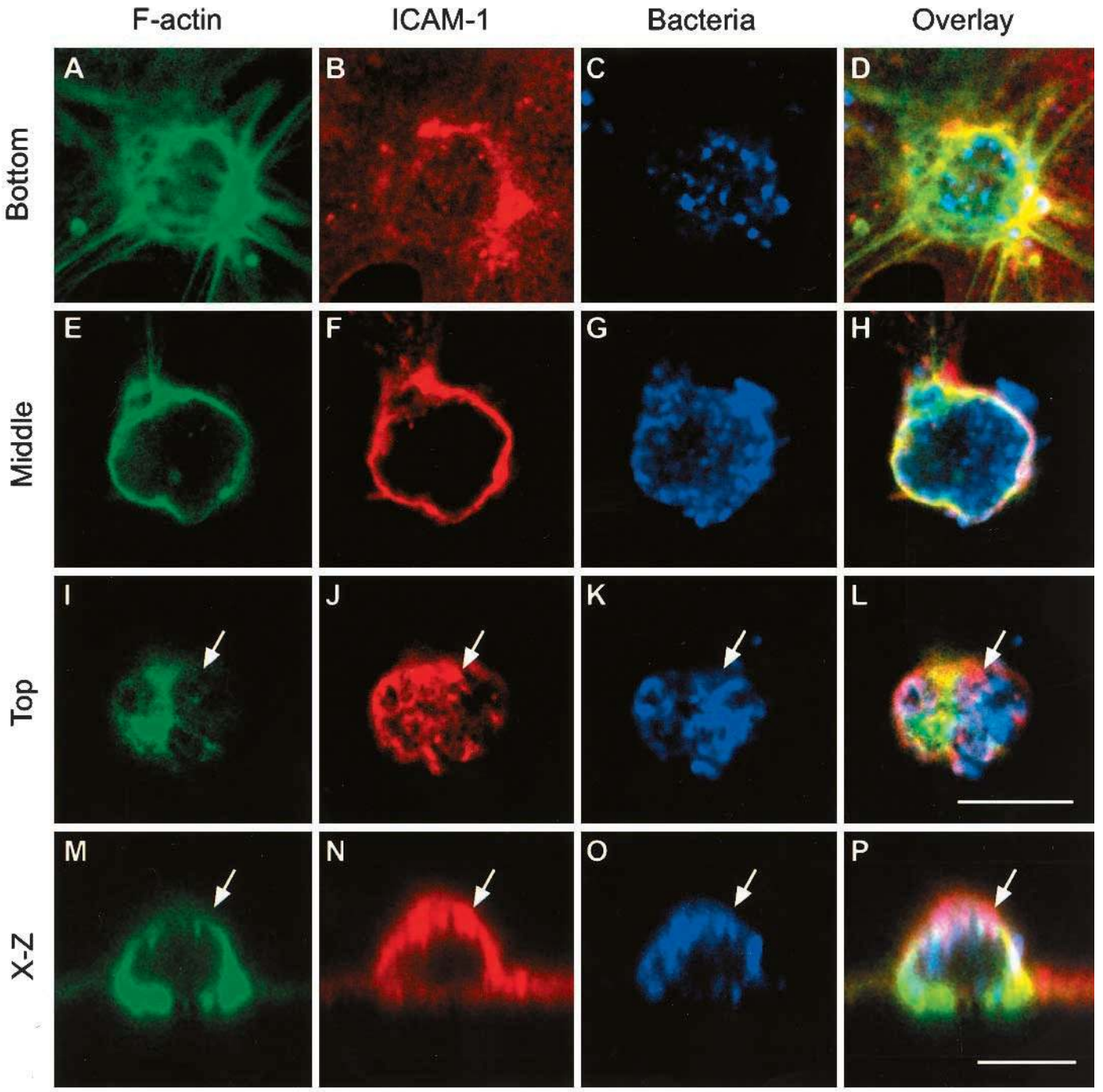

Fig. 7. Confocal microscopic analysis of the differential accumulation of ICAM-1 and submembranous F-actin in the invasome structure. HUVECs were infected with *B. henselae* strain ATCC 49793 for 48 hours, washed and fixed with formaldehyde. Specimens were stained for F-actin by FITC-labelled phalloidin (A,E,I,M) or by indirect immunofluorescence staining with monoclonal anti-ICAM-1 antibodies (B,F,J,N) and anti-*B. henselae* antiserum (C,G,K,O). Samples were analysed by confocal laser scanning microscopy. An overlay of all three channels is presented in D,H,L,P. Three consecutive optical sections in the *x-y* plane were taken from an invasome at the level of the attachment structure (A-D; bottom), or the middle part (E-H; middle) or top part (I-L; top) of the membrane protrusions engulfing the bacterial aggregate with 3 µm spacing in between adjacent layers. An *x-z* plane of an invasome structure is presented in M-P. Arrows point to ICAM-1 labelling distributed to the tips of membrane protrusions. Bars: 10 µm (A-L and M-P).

bright, F-actin staining (Figs 1D, 7A, 8A, 9G and 10A), which appears to result from actin stress fibres being twisted around the base of the invasome and extending further outside of the structure. Staining with anti-phosphotyrosine antibodies demonstrated that these stress fibres anchor the invasome structure to numerous focal adhesion plaques found in close spatial association (Fig. 8A-C, arrows). The high number of invasome-associated focal adhesion plaques may suggest that

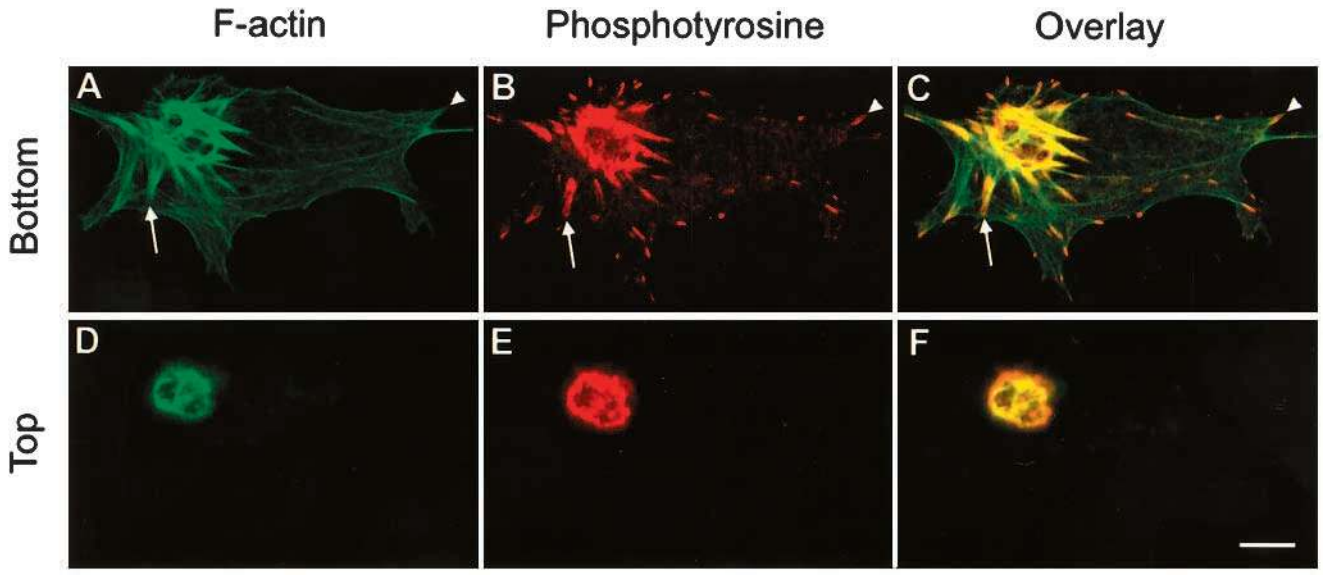

Fig. 8. Confocal microscopic analysis of F-actin and phosphotyrosine rearrangements related to the invasome structure. HUVECs were infected with *B. henselae* strain ATCC 49793 for 48 hours, washed and fixed with formaldehyde. Specimens were stained for F-actin with FITC-phalloidin (A,D; green channel) or for phosphotyrosine by indirect immunofluorescence labelling with monoclonal antibodies directed against phosphotyrosine (B,E; red channel) and specimens were analysed by confocal laser scanning microscopy. In the overlay of the two channels presented (C,F), the yellow colour indicates a colocalisation of F-actin and phosphotyrosine. Two consecutive optical sections in the x-y plane were taken at the level of actin stress fibres (A-C; bottom) or 3 μM above (D-F; top), respectively. Bar, 10 μm.

the invasome attaches more firmly to the cell substratum than do other parts of the cell (Fig. 8B,C). In consequence, a revolving locomotion of the cell would be retarded by this firmly attached invasome, which may explain the twisting of actin cables around the basal part of the invasome. This model is consistent with preliminary time-lapse microcinematography experiments indicating a quicker revolving locomotion of the leading edge relative to the invasome structure (data not shown).

Invasome-mediated invasion is actin-dependent and microtubuli-independent

In order to characterise the cytoskeletal components involved in invasome-mediated invasion, we tested for the effects of several drugs impairing cytoskeletal functions. Drugs known to cause depolymerisation of microtubuli, e.g. nocodazole (Margolis and Wilson, 1977) and colchicine (Beebe et al., 1979) did not affect the efficiency of invasome-mediated invasion as measured by quantifying three sequential stages of invasome formation (Fig. 9A,B). Immunocytochemical staining demonstrated the effectiveness of the treatment with these drugs as seen by a nearly complete depolymerisation of microtubules (Fig. 9, compare D,E with untreated cells in G). The microtubuli-stabilising drug taxol (Schiff and Horwitz, 1980) showed a mild inhibitory effect on invasome formation only when applied at high concentrations (>5 μM, Fig. 9C,F).

In contrast, the F-actin depolymerising drug cytochalasin D (Sampath and Pollard, 1991) caused a concentration-dependent inhibition of invasome formation (Fig. 10G). While bacteria still aggregated on the cell surface (Fig. 10E,F), the subsequent engulfment and internalisation of the aggregate by membrane protrusions was inhibited (Fig. 10G). The cell surface associated bacterial clumps were often associated with aggregated F-actin (Fig. 10D,E), suggesting that actin nucleation still occurred but did not allow the formation of membrane protrusions resulting in the organisation of an invasome structure.

In conclusion, invasome-mediated invasion is an F-actin-dependent and microtubule-independent process.

DISCUSSION

Invasive bacterial pathogens exploit various cellular processes to facilitate their uptake into an intracellular compartment of the host cell. Well established paradigms of invasion into epithelial cells involve the zipper-like phagocytosis of *Yersinia enterocolitica* (reviewed by Isberg and Tran Van Nhieu, 1994), *Neisseria gonorrhoeae* (reviewed by Meyer et al., 1995) and *Listeria monocytogenes* (Mengaud et al., 1996) and the uptake of *Salmonella typhimurium* and *Shigella flexneri* by macropinocytosis (Francis et al., 1993, reviewed by Ménard et al., 1996). A common scheme in these different cell invasion mechanisms is that single bacteria trigger rearrangements of the actin cytoskeleton, which leads to bacterial internalisation into an endosomal compartment within minutes or hours. *B. henselae* is a newly recognised human pathogen which has been shown to enter cultured epithelial cells by a mechanism sharing these common characteristics of cell invasion (Batterman et al. 1995, Zbinden et al. 1995). We have extended the analysis of *B. henselae* cell invasiveness to endothelial cells, which are considered to be an important cell type for the pathogenicity of *B. henselae*. Similar to epithelial cells, we have observed entry of *B. henselae* into HUVECs within several hours of infection giving rise to intracellular bacteria residing in perinuclear localising phagosomes (unpublished results). Here we describe a novel mechanism of endothelial

cell invasion by *B. henselae*, which occurs in a day rather than hours, involving a series of specific host cell-pathogen interactions. This process can be divided into three phases: (i) the accumulation and aggregation of bacteria on the cell surface, (ii) the engulfment and (iii) the internalisation of the formed bacterial aggregate by a well-organised structure, the invasome. Time-lapse microcinematography has implicated a role for the leading lamella in the process of cell surface accumulation and aggregation of *B. henselae*. The leading lamellae was found to establish contact to bacteria sedimented to the substratum, and the interacting bacteria were found to be transported rearward across the leading lamella to a site just ahead of the nucleus. This capping phenomenon is a characteristic feature of cell locomotory activity, which was studied in most detail by the movement of particles bound to the leading lamella of fibroblasts (Holifield et al., 1991; reviewed by Heath and Holifield, 1991). However, cell surface accumulation and aggregation of *B. henselae* by this capping process is not sufficient to trigger invasome-mediated internalisation. This conclusion is based on the phenotypic analysis of a spontaneous rifampicin-resistant mutant strain of *B. henselae* (Dehio and Meyer, 1997), which was coincidentally found to be impaired in invasome-mediated internalisation. At an early stage of infection, cell surface accumulation of

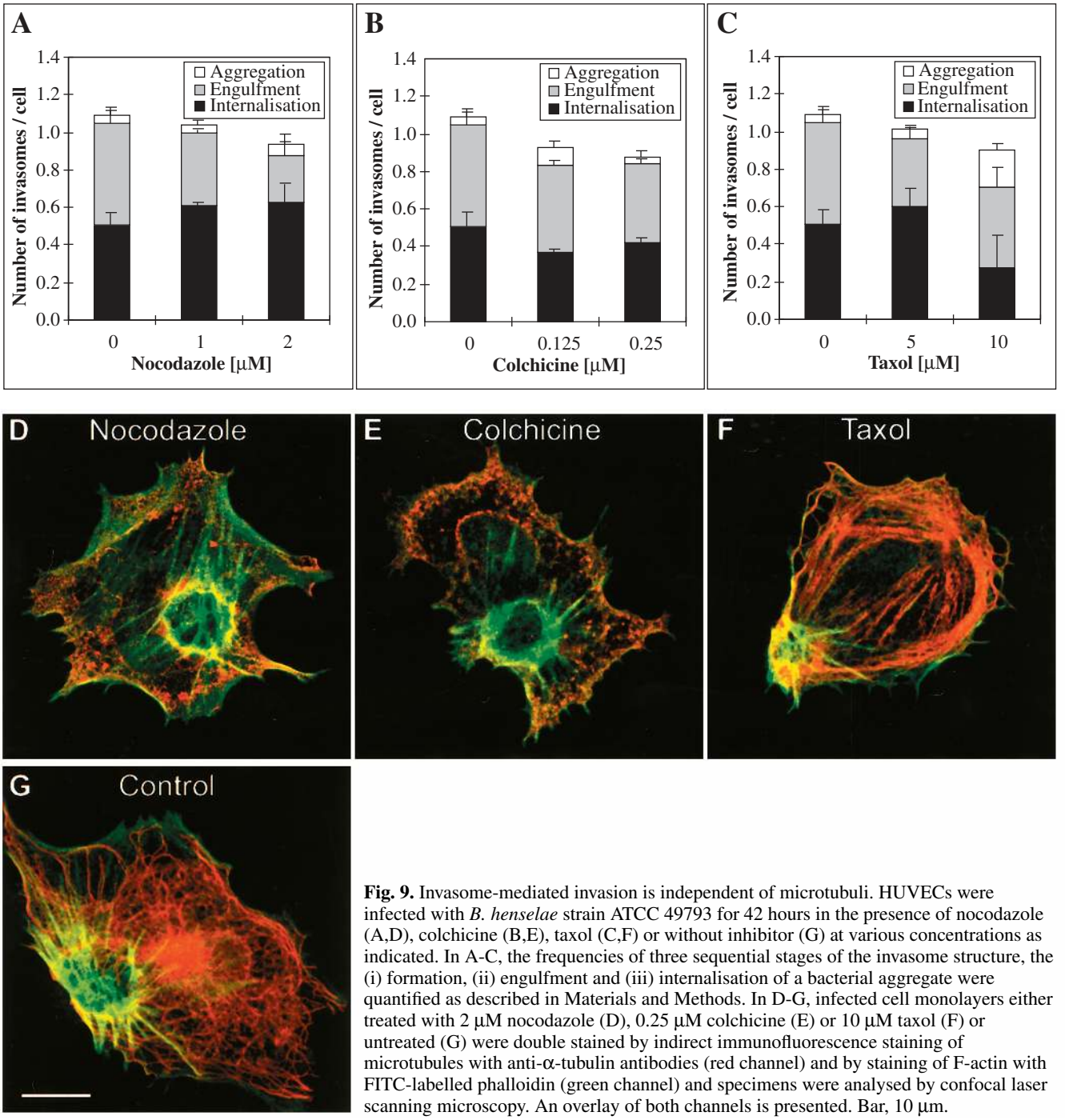

Fig. 9. Invasome-mediated invasion is independent of microtubuli. HUVECs were infected with *B. henselae* strain ATCC 49793 for 42 hours in the presence of nocodazole (A,D), colchicine (B,E), taxol (C,F) or without inhibitor (G) at various concentrations as indicated. In A-C, the frequencies of three sequential stages of the invasome structure, the (i) formation, (ii) engulfment and (iii) internalisation of a bacterial aggregate were quantified as described in Materials and Methods. In D-G, infected cell monolayers either treated with 2 μM nocodazole (D), 0.25 μM colchicine (E) or 10 μM taxol (F) or untreated (G) were double stained by indirect immunofluorescence staining of microtubules with anti-α-tubulin antibodies (red channel) and by staining of F-actin with FITC-labelled phalloidin (green channel) and specimens were analysed by confocal laser scanning microscopy. An overlay of both channels is presented. Bar, 10 μm.

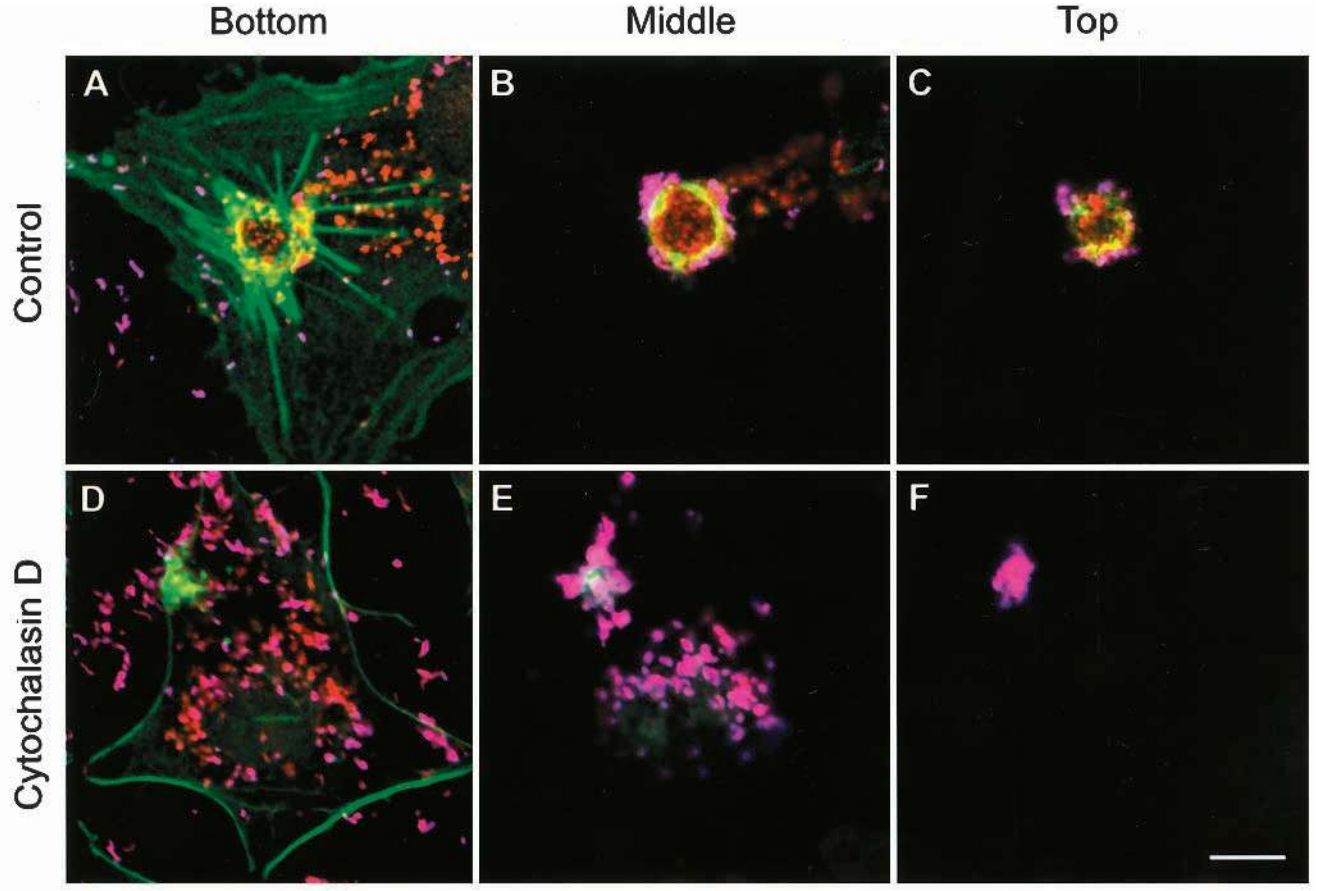

Fig. 10. Invasome-mediated invasion is actin-dependent. HUVECs were infected with *B. henselae* strain ATCC 49793 for 42 hours in the absence (A-C,G) or presence of cytochalasin D at 100 nM (D-F) or at various concentrations as indicated (G). In A-F, infected cell monolayers were stained for extracellular bacteria (before host cell membrane permeabilisation, blue channel) or the totality of bacteria (after host cell membrane permeabilisation, red channel) by indirect immunofluorescence staining and F-actin was stained by FITC-labelled phalloidin (green channel) and specimens were analysed by confocal laser scanning microscopy. An overlay of all three channels is presented in which intracellular bacteria appear in red and extracellular bacteria in purple, and a colocalisation of intracellular bacteria and F-actin appears in yellow. Three consecutive optical sections taken at the level of the stress fibres (A,D; bottom), or spaced by 2.5 μM (B,E; middle) or 5 μM (C,F; top), respectively, are shown. Bar, 10 μm. In G, the frequencies of three sequential stages of the invasome structure, the (i) formation, (ii) engulfment and (iii) internalisation of a bacterial aggregate were quantified as described in Materials and Methods.

bacteria from this mutant strain was virtually indistinguishable to that of the invasome-forming clinically isolated progenitor strain. Interestingly, the mutant strain subsequently showed an increased level of bacterial uptake by a process similar to bacterial entry into epithelial cells, suggesting that invasome-mediated internalisation interferes with alternative mechanisms of bacterial entry into endothelial cells. The genetic basis for the deficiency in invasome-mediated invasion exerted by the rifampicin-resistant mutant strain is presently unknown. The identification and characterisation of the affected bacterial factor(s) critical for invasome-mediated invasion may be facilitated by the recent development of genetic tools which allow the manipulation of *B. henselae* (Dehio and Meyer, 1997).

Subsequent to the accumulation and aggregation of bacteria on the cell surface, the invasome is formed. We have used various microscopic techniques to describe in detail this process encompassing the engulfment and internalisation of the bacterial aggregate. Engulfment of the bacterial aggregate appears to result from a circular outgrowth of membrane protrusions from the cell contact area with the associated bacterial aggregate. Membrane protrusions extending to the top of the bacterial aggregate finally fuse with each other resulting in the complete internalisation of the bacterial aggregate. In this

respect, it was intriguing to find enrichment for the intercellular adhesion molecule-1 (ICAM-1) in the membrane protrusions formed, particularly distributing to their tips. ICAM-1 is well known to mediate interaction with lymphocyte function-associated antigen 1 (LFA-1), which results in intercellular adhesion of endothelial cells and leukocytes (Marlin and Springer, 1987). Similarly, *B. henselae*-expressed ligands may also interact with ICAM-1, which may be suggested by the firm interaction of the tips of membrane protrusions enriched for ICAM-1 with the underlying bacterial aggregate. This distribution of ICAM-1, however, is also reminiscent of the accumulation of ICAM-1 at the tip of the uropod, which represents a well-defined cytoplasmic projection formed during T-cell activation (del Pozo et al., 1995). The clarification of the role of ICAM-1 in invasome-mediated invasion therefore awaits further experimental analysis.

Submembranous F-actin as well as phosphotyrosine were also found to accumulate in the membrane protrusions of the invasome structure, although both components did not accumulate at the tip of the protrusions as demonstrated for ICAM-1. Rearrangement of the actin cytoskeleton plays a crucial role in cell invasion by *Shigella flexneri* (Clerc and Sansonetti, 1987), *Salmonella typhimurium* (Finlay and Falkow, 1988), *Yersinia enterocolitica* (Finlay and Falkow, 1988) and enteropathogenic *Escherichia coli* (Donnenberg et al., 1990) as shown both by phalloidin-staining characteristics and cytochalasin D sensitivity of these cellular invasion processes. Rearrangements of the actin cytoskeleton is also crucial for invasome-mediated internalisation, since cytochalasin D treatment was found to inhibit the formation of membrane protrusions which may engulf and internalise the cell surface located bacterial aggregate as seen in untreated cells. In contrast, drugs either depolymerising or stabilising microtubules did not affect invasome formation.

The co-accumulation of phosphotyrosine and submembranous F-actin in membrane protrusion of the invasome is indicative of cellular signalling processes associated with cytoskeletal rearrangements, similar to that reported for cell invasion by enteropathogenic *Escherichia coli* (Rosenshine et al., 1992a) and *Shigella flexneri* (Dehio et al., 1995). Protein tyrosine kinase inhibitors have previously been used to block cell invasion processes by other bacteria (Rosenshine et al., 1992b). To clarify the role of tyrosine phosphorylation for invasome-mediated internalisation, however, the careful use of these inhibitor compounds might be critical due to toxic side effects associated with the long duration of treatment necessary for this model system.

In addition to submembranous cortical F-actin found in the membrane protrusions, the invasome structure is also associated with rearrangements of stress fibres. Interestingly, numerous actin stress fibres were found to be twisted around the basal part of the invasome as well as being anchored to invasome-associated focal adhesion plaques. The increased number of invasome-associated focal adhesion plaques may suggest that the invasome attaches more firmly to the cell substratum than to other parts of the cell. In consequence, a revolving locomotion of the cell would be retarded by this firmly attached invasome, which may explain the twisting of actin cables around the basal part of the invasome. In favour of this model, preliminary microcinematographic observation indicated a slower revolving locomotion of the invasome relative to the leading edge of the cell (data not shown). The dynamics of the cellular locomotion process could be viewed in analogy to the dynamics of a hurricane, with the invasome being represented by the eye of the hurricane. By this model, twisting forces would also explain the evenly round structure of the invasome and the bacterial aggregate residing within. Final proof of this model awaits long term and high resolution time-lapse video microscopy.

The in vitro characteristics of invasome-mediated internalisation of *B. henselae* into endothelial cells suggest a role for this process in the invasion or colonisation of endothelial cells in vivo. The colonisation of vascular tissues is indeed an important aspect in *B. henselae* pathogenicity, which results in vaso-proliferative tumour growth. Interestingly, the atypically proliferating endothelial cells appear to be firmly associated with clumps of *B. henselae*, although ultrastructural data suggest that these bacteria are primarily extracellular (Schneider et al., 1993; Hettmansperger et al., 1993; Monteil et al., 1994). Refined histological and ultrastructural analysis may indicate if invasomes are formed in these tumour lesions or other tissue pathologies associated with *B. henselae* infection.

Although the significance of invasome formation in *B. henselae* pathogenesis is still unknown, we have described in this report a novel cellular process which mediates bacterial invasion. Further analysis of the mechanisms of cellular locomotion and membrane trafficking involved will be required to fully unravel how *B. henselae* may trigger its internalisation by the invasome structure. One may expect that these studies will also allow us to gain new insights into some basic, but elusive, aspects of endothelial cell biology.

We are particularly grateful to Dr Thomas Meyer for his support and interest in this work. We thank Dr Ingo Authenrieth and Dr Burt Anderson for providing *B. henselae* strains. We are grateful to Dr Dorian Haskard for anti-ICAM-1 antibodies. We thank Dr Ludwig Kiesel and Regina Fendt for providing umbilical cords and Anja Haude for excellent technical assistance in cell culture and Josette Arondel for help in preparing anti-*B. henselae* antisera. We thank Dr Scott Gray-Owen and Michaela Dehio for critical reading of the manuscript.

REFERENCES

Adal, K. A., Cockerell, C. J. and Petri, W. A. (1994). Cat scratch disease, bacillary angiomatosis, and other infections due to *Rochalimaea*. *N. Engl. J. Med.* **330**, 1509-1515.

Autrata, R., Hermann, R. and Muller, M. (1992). An efficient single crystal BSE detector in SEM. *Scanning* **14**, 127-135.

Batterman, H. J., Peek, J. A., Loutit, J. S., Falkow, S. and Tompkins, L. S. (1995). *Bartonella henselae* and *Bartonella quintana* adherence to and entry into cultured human epithelial cells. *Infect. Immun.* **63**, 4553-4556.

Beebe, D. C., Feagans, D. E., Blanchette-Mackie, E. J. and Nau, M. E. (1979). Lens epithelial cell elongation in the absence of microtubules: evidence for a new effect of colchicine. *Science* **206**, 836-838.

Brenner, D. J., O'Connor, S. P., Winkler, H. H. and Steigerwalt, A. G. (1993). Proposals to unify the genera *Bartonella* and *Rochalimaea*, with descriptions of *Bartonella quintana* comb. nov., *Bartonella vinsonii* comb. nov., *Bartonella henselae* comb. nov., and *Bartonella elizabethae* comb. nov., and to remove the family *Bartonellaceae* form the order Rickettsiales. *Intern. J. Syst. Bacteriol*. **43**, 777-786.

Conley, T., Slater, L. and Hamilton, K. (1994). *Rochalimaea* species stimulate human endothelial cell proliferation and migration *in vitro*. *J. Lab. Clin. Med.* **124**, 521-528.

Clerc, P. and Sansonetti, P. J. (1987). Entry of *Shigella flexneri* into HeLa cells: evidence for directed phagocytosis involving actin polymerization and myosin accumulation. *Infect. Immun.* **55**, 2681-2688.

Danscher, G. (1981). Localization of gold in biological tissue. A photochemical method for light and electronmicroscopy. *Histochemistry* **71**, 81-88.

Dehio, C., Prévost, M.-C. and Sansonetti, P. (1995). Invasion of epithelial cells by *Shigella flexneri* induces tyrosine phosphorylation of cortactin by a pp60$^{c\text{-}src}$-mediated signalling pathway. *EMBO J.* **14**, 2471-2482.

Dehio, C. and Meyer, M. (1997). Maintenance of broad-host-range incompatibility group P and group Q plasmids and transposition of Tn5 in *Bartonella henselae* following conjugal plasmid transfer from *Escherichia coli*. *J. Bacteriol.* **179**, 538-540.

del Pozo, M. A., Sanchez-Mateos, P., Nieto, M. and Sanchez-Madrid F. (1995). Chemokines regulate cellular polarization and adhesion receptor redistribution during lymphocyte interaction with endothelium and extracellular matrix. *J. Cell. Biol.* **131**, 495-508.

Donnenberg, M. S., Donohue-Rolfe, A. and Keusch, G. T. (1990). A comparison of Hep-2 cell invasion by enteropathogenic and enteroinvasive *Escherichia coli*. *FEMS Microbiol. Lett.* **57**, 83-86.

Finlay, B. B. and Falkow, S. (1988). A comparison of microbial invasion strategies of *Salmonella*, *Shigella* and *Yersinia* species. *Mol. Cell. Biol.* **64**, 227-243.

Francis, C. L., Ryan, T. A., Jones, B. D., Smith, S. J. and Falkow, S. (1993). Ruffles induced by *Salmonella* and other stimuli direct macropinocytosis of bacteria. *Nature* **364**, 639-642.

Heath, J. P. and Holifield, B. F. (1991). Cell locomotion: new research tests old ideas on membrane and cytoskeletal flow. *Cell Motil. Cytoskel.* **18**, 245-257.

Hettmannsperger, U., Soehnchen, R., Gollnick, H., Detmar, M. and Orfanos, C. E. (1993). Bazilläre epithelioide Angiomatose bei fortgeschrittener HIV-Infektion. *Hautarzt* **44**, 803-807.

Holifield, B. F., Ishihara, A. and Jacobson, K. (1991). Comparative behavior of membrane protein-antibody complexes on motile fibroblasts: implication for a mechanism of capping. *J. Cell Biol.* **111**, 2499-2512.

Isberg, R. R. and Tran Van Nhieu, G. (1994). Binding and internalization of microorganisms by integrin receptors. *Trends Microbiol.* **2**, 10-14.

Koehler, J. and Tappero, W. (1993). Bacillary angiomatosis and bacillary peliosis in patients infected with human immunodeficiency virus. *Clin. Infect. Dis.* **17**, 612-624.

Lucey, D., Dolan, M. J., Moss, C. W., Garcia, M., Hollis, D. G., Wenger, S., Morgan, G., Almeida, R., Leong, D., Greisen, K. S., Welch, D. F. and Slater, L. N. (1992). Relapsing illness due to *Rochalimaea henselae* in immunocompetent hosts: implication for therapy and new epidemiological associations. *Clin Inf. Dis.* **14**, 683-688.

Margolis, R. L. and Wilson, L. (1977). Addition of colchicine-tublin complex to microtubule ends: the mechanism of substoichiometic colchicine poisoning. *Proc. Nat. Acad. Sci. USA* **74**, 3466-3470.

Marlin, S. D. and Springer, T. A. (1987). Purified intercellular adhesion molecule-1 (ICAM-1) is a ligand for lymphocyte function-associated antigen 1 (LFA-1). *Cell* **51**, 813-819.

Ménard, R., Dehio, C. and Sansonetti, P. (1996). Bacterial entry into epithelial cells: The paradigm of *Shigella. Trends Microbiol.* **4**, 220-226.

Mengaud, J., Ohayon, H., Gounon, P., Mège, R.-M. and Cossart, P. (1996). E-cadherin is the receptor for internalin, a surface protein required for entry of *L. monocytogenes* into epithelial cells. *Cell* **84**, 923-932.

Meyer, T. F., Pohlner, J. and van Putten, J. P. M. (1995). Biology of the pathogenic *Neisseriae*. In *Current Topics in Microbiology and Immunology, Vol. 192: Bacteria pathogenesis of plants and animals* (ed. J. L. Dangl), pp. 283-318. Springer-Verlag, Berlin.

Monteil, R. A., Michiels, J.-F., Hofman, P., Saint-Paul, M.-C., Hitzig, C., Perrin C. and Santini, J. (1994). Histological and ultrastructural study of one case of oral bacillary angiomatosis in HIV disease and review of the literature. *Oral Oncol., Eur. J. Cancer* **30B**, 65-71.

Regnery, R. L., Anderson, B. E., Clarridge III, J. E., Rodriguez-Barradas, M. C., Jones, D. C. andCarr, J. H. (1992). Characterization of a novel *Rochalimaea* species, *R. henselae* sp. nov., isolated from blood of a febrile, human immunodeficiency virus-positive patient. *J. Clin. Microbiol.* **30**, 265-274.

Rosenshine, I., Donnenberg, M. S., Kaper, J. B. and Finlay, B. B. (1992a). Signal transdution between enteropathogenic *Escherichia coli* (EPEC) and epithelial cells: EPEC induces tyrosine phosphorylation of host cell proteins to initiate cytoskeletal rearrangement and bacterial uptake. *EMBO J.* **11**, 3551-3560.

Rosenshine, I., Duronio, V. and Finlay, B. B. (1992b). Tyrosine protein kinase inhibitors block invasin-promoted bacterial uptake by epithelial cells. *Infect. Immun.* **60**, 2211-2217.

Sampath, P. and Pollard, T. D. (1991). Effects of cytochalasin, phalloidin, and pH on the elongation of actin filaments. *Biochemistry* **30**, 1973-1980.

Schiff, P. B. and Horwitz, S. B. (1980). Taxol stabilizes microtubules in mouse fibroblast cells. *Proc. Nat. Acad. Sci. USA* **77**, 1561-1565.

Schneider T., Ullrich, R., Schmitt-Gräff, A., Bergs, C., Reiterer, L., Dissmann, T., Zeitz, M. and Riecken, E. O. (1993). Bacillary angiomatosis in a German patient with AIDS. *Clin. Investig.* **72**, 50-54.

Webster G. F., Cockerell, C. J. and Friedman-Kien, A. E. (1992). The clinical spectrum of bacillary angiomatosis. *Br. J. Dermatol.* **126**, 535-541.

Welch, D. F., Pickett, D. A., Slater, L. N., Steigerwalt, A. G. and Brenner, D. J. (1992). *Rochalimaea henselae* sp. nov., a cause of septicemia, bacillary angiomatosis, and parenchymal bacillary peliosis. *J. Clin. Microbiol.* **30**, 275-280.

Zbinden, R., Höchli, M. and Nadal, D. (1995). Intracellular location of *Bartonella henselae* cocultivated with Vero cells and used for indirect fluorescent-antibody test. *Clin. Diag. Lab. Immun.* **2**, 693-695.

(Received 2 January 1997 – Accepted 4 July 1997)